Journal of Coastal Research	5	3	391-401	Charlottesville, Virginia	Summer 1989

Turbidity-Induced Sedimentation in Closed-End Channels

Chung-Po Lin[a] **and Ashish J. Mehta**

Coastal and Oceanographic Engineering Department
University of Florida
Gainesville, FL 32611

ABSTRACT

LIN, C. P. and MEHTA, A. J., 1989. Turbidity-induced sedimentation in closed-up channels. *Journal of Coastal Research*, 5(3), 391-401. Charlottesville (Virginia). ISSN 0749-0208.

The mechanism by which turbidity currents propagate and cause sedimentation in closed-end channels such as pier slips and residential canals was studied in laboratory experiments. Two similar flumes were used, each consisting of a main channel carrying fine-grained sediment-laden flow and an orthogonally placed closed-end channel with a gated entrance. Characteristics of the turbidity current and sediment deposition in the closed-end channel were investigated following gate opening. Behavioral similarities as well as basic differences between turbidity current and non-settling gravity currents were observed. Several properties, *e.g.* suspension concentration, showed exponential-type decay with distance. The ratio of sediment settling velocity to the densimetric velocity was found to be a significant parameter for comparing results from tests using different sediments. Sediment influx rate through the entrance was found to be proportional to 3/2 power of suspension concentration at the entrance. This relationship yields a simple method to calculate the amount of sedimentation in the channel.

ADDITIONAL INDEX WORDS: *Closed-end channels, fine-grained sediments, sediment deposition, turbidity currents.*

INTRODUCTION

Closed-end channels such as pier slips, tidal docks, elongated marinas and residential canals are well known sites for fine-grained sediment deposition. For example, in an investigation of the pier slips at the Mare Island Naval Shipyard in the San Francisco Bay area, JENKINS *et al.* (1980) found the rate of sedimentation in the slips to be as much as 2.5 times higher than that in the main channel to which the slips were connected.

In general, advective transport due to the tidal prism, wind-driven circulation and density-induced currents are mechanisms by which sediment enters the closed-end channel. Turbidity current is driven by the difference in density between the sediment-laden outside waters and the relatively quiescent and sediment-free waters in the channel. With reference to sediment transport this current can be eroding or depositional, or it can be in the form of an autosuspension (AKIYAMA and STEFAN, 1985). Turbidity current of interest to this study was of the depositional type, with virtually no resuspension.

The contribution to the total rate of sedimentation from this mechanism varies with the physical conditions. In areas where tides are weak or when the suspended sediment concentration is high, turbidity current becomes an important source of sediment in the channel (McDOWELL, 1971). For example in many residential canals in Florida, sedimentation largely occurs during storms when the suspended sediment concentration in the waterways increases by one to three orders of magnitude over that during fair weather (MEHTA and MAA, 1985). Sediment influx under these conditions can be thought of as occurring in "bursts" separated in time by relatively low level ambient concentrations (5–10 mgL^{-1}). Prototype observations of sedimentation in closed-end canals in southern Florida seem to support such episodic sediment transport characteristics (WANLESS, 1975).

A strong motivating factor for carrying out this study was the desire to understand the turbidity current as one of the mechanisms responsible for sedimentation in residential canals such as those found in Florida. However, the

88008 received 8 February 1988, accepted in revision 22 November 1988.

[a] *Present address: Coastal Technology Corporation, 1501 Sunset Drive, Suite 3, Coral Gables, FL 33143*

approach selected was focussed on the mechanism of stratified flow which governs the propagation of turbidity current and the rate of sedimentation. Prior observations (McDOWELL, 1971; GOLE *et al.*, 1973), although of a limited nature, provided the initial physical framework for organizing the study. By using a wide range of fine-grained sediments, an effort was made to identify specific sediment-related parameters which influence turbidity transport.

Laboratory experiments were conducted in two similar systems, each consisting of a closed-end channel connected orthogonally to a main channel carrying sediment-laden flow. A gate was provided at the entrance to the closed-end channel. The gate was closed initially with equal water levels on both sides, but without sediment in the closed-end channel. The behaviors of the propagating front and sediment deposition were then investigated. It is convenient to view the gate opening procedure as analogous to the generation of a relatively high concentration front during a storm. Results from a series of tests highlighting the basic physical processes under such conditions are described in this paper.

BACKGROUND

A closed-end channel of length L and width B orthogonally connected to the main channel, and a turbidity front of instantaneous length x_f measured from the entrance ($x = 0$), are shown in Figures 1a, b. The mean depth of water is H above the horizontal bottom ($z = 0$). The sediment-laden flow in the main channel is fully turbulent and vertically well-mixed. The fluid density there is $\rho_w + \Delta\rho_o$, where ρ_w is the clear water density and $\Delta\rho_o$ is the density increment due to suspended sediment. Immediately inside the entrance a gyre zone occurs in which circulation is driven by the lateral shear due to the main channel flow. The horizontally and vertically mixed flow is weakly turbulent, and the distance of influence of the gyre is limited, being of the same order as channel width B. Also almost immediately inside the entrance, deposition of sediment commences and the suspension density there, $\rho_w + \Delta\rho_1$, is lower than that in the main channel. The density increment, $\Delta\rho_1$, is therefore characteristically lower than $\Delta\rho_o$. It was found that for most of the phenomena observed, $\Delta\rho_1$ was better representative of the driving force of turbidity current than $\Delta\rho_o$. Beyond the gyre the flow is predominantly viscous and stratified, with a clearly identifiable interface ($z = \eta$). Three characteristic features of the front are the nose ($z = h_1$), the head (h_2) and the neck (h_3) (SIMPSON, 1972).

Another characteristic feature of the front is that in a sufficiently long channel, front motion eventually slows down and the front ultimately becomes stationary at a distance where the finest particles in suspension settle out. The fluid density decreases up to the front, where it almost equals that of clear water. A steady state occurs, and there is an overall balance of forces including the depth-integrated excess gravity force, water level set up in the channel and bottom friction. However, due to a local force imbalance at every elevation above the bottom, sediment-laden water continues to enter through the lower half of the water column at the entrance, while an equal volume per unit time of almost sediment-free water leaves from the upper half. This undercurrent is the cause of sedimentation in the channel.

Three noteworthy aspects of the phenomenon examined were: (1) the transient behavior of the propagating front after gate opening, (2) characteristics of the stationary front, and (3) rate of sedimentation. In order to elucidate the physical mechanisms, three approaches were selected: (1) dimensional analysis for organizing the experimental data, (2) numerical modeling to examine the transient and stationary front behaviors, and (3) analytic approaches to examine the stationary front behavior. These approaches are summarized below.

Dimensional Analysis

Dimensionless groups were developed via the well known π-theorem for treating data on the characteristics of the propagating as well as stationary fronts (LOTT, 1986; LIN, 1987). While it was not practical to evaluate the effect of each group on front behavior, this type of analysis mainly highlighted the significance of the important parameters in governing transport. Thus for example the front speed, u_f, can be expressed as

$$\frac{u_f}{u_\Delta} = f\left(\frac{x}{H}, \frac{B}{H}, \frac{u_\Delta H}{\nu}, \frac{w_s}{u_\Delta}\right) \qquad (1)$$

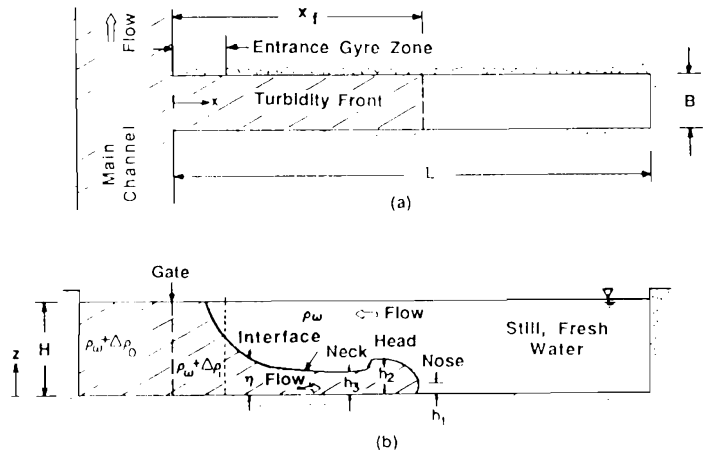

Figure 1. Turbidity front in a closed-end channel: (a) plan, (b) side view.

where ν is the kinematic viscosity of the fluid and w_s is the sediment settling velocity. Furthermore, $u_\Delta = (g\,H\,\Delta\rho_1/\rho_w)^{1/2}$, where g is acceleration due to gravity, is the densimetric velocity (BARR, 1963). Equation 1 indicates that the dimensionless front speed depends on the front position, x/H, channel aspect ratio, B/H, densimetric Reynolds number, $Re_\Delta = u_\Delta H/\nu$, and the relative settling velocity, w_s/u_Δ. This relationship is analogous to that for the speed of the saline front advancing against river flow of velocity u_r. In that case w_s is replaced by u_r (KEULEGAN, 1966).

Numerical Modeling

A time varying, two-dimensional (x,z), finite-difference mathematical model was developed to simulate the flow and suspension concentration fields in the closed-end channel. This model is based on the equations of flow continuity, momentum and sediment mass conservation as follows:

$$\frac{\partial u}{\partial x} + \frac{\partial w}{\partial z} = 0 \qquad (2)$$

$$\frac{\partial u}{\partial t} + \frac{\partial u^2}{\partial x} + \frac{\partial (uw)}{\partial z} = -\frac{1}{\rho}\frac{\partial p}{\partial x} + \frac{\partial}{\partial x}\left(e_x \frac{\partial u}{\partial x}\right) + \frac{\partial}{\partial z}\left(e_z \frac{\partial u}{\partial z}\right) \qquad (3)$$

$$0 = -g - \frac{1}{\rho}\frac{\partial p}{\partial z} \qquad (4)$$

$$\frac{\partial C}{\partial t} + \frac{\partial (uC)}{\partial x} + \frac{\partial}{\partial z}[(w - w_s)C] = \frac{\partial}{\partial z}\left(\epsilon_x \frac{\partial C}{\partial x}\right) + \frac{\partial}{\partial z}\left(\epsilon_z \frac{\partial C}{\partial z}\right) - d \qquad (5)$$

where u, w are velocity components in the x and z directions, respectively; ρ is fluid density; p is pressure; e_x, e_z, ϵ_x, ϵ_z are momentum and mass diffusion coefficients in the x and z directions, respectively; and d is sediment deposition rate.

The sparse grid system (MILES, 1977) in space was employed in the finite difference formulation of these governing equations. In this formulation, an explicit numerical scheme was used and the temporal, convective, and diffusive terms in the equations were time- and space-centered (LIN, 1987). Within each time step of simulation, the velocity field was first solved based on the flow continuity and momentum equations (Eqs. 2-4). The resulting flow field was then applied to determine the magnitude of convective transport of suspended sediment, and further to solve for the time-varying sediment concentration distribution based on the mass conservation equation.

Boundary conditions required to solve the governing equations include: (1) zero shear stress and no mass flux of suspended sediment at the water surface; (2) no flow or mass flux through the channel bottom and the closed-end; and (3) a given sediment concentration profile and water surface elevation at the channel entrance.

The coefficients in the model were flow and/or sediment concentration dependent, and were determined by model calibration and direct laboratory measurements. Data from test COEL-4 were used for model calibration. The validity of Reynolds analogy between diffusive momentum and mass transports for fine-grained sediment was assumed (JOBSON and SAYRE, 1970). As a result of calibration, it was found that $e_x = \epsilon_x = 5 \times 10^{-3}$ m^{2}s^{-1}, and $e_z = \epsilon_z = 10^{-6}$ m^{2}s^{-1}. In addition, Manning's n for bed roughness was found to be 0.03, which was close to that obtained from the Moody diagram for the corresponding flow Reynolds number.

Two deposition-related parameters for fine-grained sediments, the settling velocity, w_s, and the critical stress for deposition, τ_{cd}, were determined by independent laboratory measurements. The median (by weight) settling velocity of fine-grained sediments varies with sediment concentration. The derivation of such an empirical relationship for specific sediment requires an independent set of tests in a settling column (LOTT, 1986). For example for kaolinite as sediment within the selected concentration range (86 to 3,746 mgL^{-1}, it was found that $w_s = 1 \times 10^{-6} C^{0.78}$, where w_s is measured in ms^{-1} and concentration, C, in mgL^{-1}. An analysis of kaolinite deposition data in the main channel yielded a value of 0.13 Nm^{-2} for the critical stress, τ_{cd}. For all the bed shear stresses, τ_b, greater than τ_{cd} no deposition was considered to occur (MEHTA and LOTT, 1987).

Data from test COEL-5 were used to verify the calibrated model. The results of model calibration and verification (LIN, 1987) showed a reasonable agreement between the model prediction and experimental data.

When applying this model to predict the flow and sediment concentration distribution in a prototype closed-end channel, similar procedures of model calibration and verification based on field data are required. However, the vertical momentum and mass diffusion coefficients need to account for buoyancy effects of stratified flow through appropriate formulations involving the gradient Richardson number (LIN, 1987).

Analytic Approach

The occurrence of a stationary front permits a simplification of the governing equations, which can then be solved to yield approximate results. An advantage these results offer over numerical ones is that they highlight the significance of the important factors in explaining observations related to the flow and concentration fields at steady state. Illustrative results are given in the following paragraphs.

Flow Velocity. A stationary front occurs under a balance between gravity and viscous forces. The length of this front can be conventionaly assumed to be considerably greater than the still water depth, H. The water layer above the front may further be considered to be sediment-free, with all the sediment confined to the lower layer with a uniform (constant) concentration. Under these conditions momentum diffusion can be shown to be much more important in the vertifical than in the horizontal direction (LIN, 1987). The closed-end causes a water surface slope to be set up, with the hydrostatic head balancing the sum of the excess pressure force due to the density gradient and the flow-induced bottom shear. In addition, inflow is balanced by outflow at every flow cross-section. Given the outflow velocity at the surface, u_s, which can be easily measured, the following expressions for the vertical profiles of the horizontal velocity, u, are obtained in the two layers:

$\xi < \zeta < 1$:

$$\frac{u}{u_s} = \frac{(1.5 - 0.375\xi)\zeta^2 - (3 - 0.75\xi)\zeta + 1}{0.375\xi - 0.5} \quad (6)$$

$0 < \zeta < \xi$:

$$\frac{u}{u_s} = \frac{(\zeta/\xi)^3 + (-3 + 1.5\xi^2}{-0.375\xi^3)(\zeta/\xi)^2 + (3 - 3\xi + 0.75\xi^2)(\zeta/\xi)} \quad (7)$$

$$0.375\xi - 0.5$$

where $\zeta = z/H$ and $\xi = \eta/H$.

Concentration in Lower Layer. The variation of the depth-mean concentration in the lower layer, $\bar{C}_b$, with distance can be examined by solving the steady state sediment mass transport equation. As a first order approximation only two terms, $u\partial\bar{C}_b/\partial x$ and $w_s\partial\bar{C}_b/\partial z$, need to be considered. Equating these terms amounts to balancing advective transport with gravitational settling. Experimental observations indicated an exponential decay of u and w_s

with distance (LIN, 1987). Therefore, $w_s = w_{s1} \exp(-\beta_1 x)$ and $u = u_1 \exp(-\beta_2 x)$ may be assumed, where subscript 1 for w_s and u refers to conditions at the entrance, and β_1, β_2 are empirical coefficients. Omitting details, the resultant relationship for $\bar{C}_b$ upon integration of the mass balance equation can be expressed as

$$\frac{\bar{C}_b}{\bar{C}_{b1}} = \exp\left[-\beta\left(\frac{w_{s1}}{u_\Delta}\right)\left(\frac{x}{H}\right)\right] \quad (8)$$

where $\bar{C}_{b1}$ is the value of $\bar{C}_b$ at the entrance, and β depends on sediment properties. Investigations of lock exchange flows involving salinity-induced gravity currents suggest $\beta > 4$ (O'BRIEN and CHERNO, 1934; YIH, 1965; LIN, 1987).

Sediment Influx. The sediment influx rate at the entrance, S, is equal to $u_1\bar{C}_1$, where $\bar{C}_1$ is the depth-mean concentration at the entrance. Experimental observations indicate that shortly after gate opening the inflow velocity, u_1, decreases from the initial front speed, u_{f1}, and approaches a constant value (GOLE *et al.*, 1973; LIN, 1987). Furthermore, it was found that u_1 is proportional to u_{f1}, and in fact $u_{f1} \sim 0.5\, u_\Delta$ has been reported by IPPEN and HARLEMAN (1952) and BENJAMIN (1968). Therefore, in general $u_1 = \alpha u_\Delta$, where α is a proportionality constant. As a result $S = \alpha u_\Delta \bar{C}_1$. Expressing $\Delta\rho_1$ (in u_Δ) in terms of $\bar{C}_1$, it follows that

$$S = \alpha\left[\frac{gH}{\rho_w}\left(1 - \frac{1}{G_s}\right)\right]^{1/2} \bar{C}_1^{3/2}$$

where G_s is the specific gravity of the sediment. It is interesting to note that for a given sediment and water depth, S is proportional to the 3/2 power of sediment concentration at the entrance.

TEST CONDITIONS

Two conceptually similar flume systems were used, one at the U.S. Army Engineer Waterways Experiment Station (WES), Vicksburg, Mississippi, and the other at the University of Florida's Coastal Engineering Laboratory (COEL). The dimensions of the closed-end channels are given in Table 1. Also given are the depth-mean concentration in the main channel, C_o, and the fluid density increment, $\Delta\rho_1$, used in all data representation and computations. A total of 13 tests were carried out at WES and 14 at COEL. The longest test duration was 276 min in test WES-13. The test-mean fluid temperature at WES ranged from 15.1 to 22.4°C, and at COEL from 18.9 to 26.7°C. Occasional difficulties were encountered during some of the tests in maintaining a constant water temperature. This resulted in undesirable although typically minor effects due to thermally-induced currents. In some tests minor oscillations in otherwise steady flow speed and suspension concentration in the main channel resulted in unavoidable data scatter.

Seven fine-grained sediments covering a range of physical and physicochemical properties were used. Some were cohesive and others nearly non-cohesive. The two cohesive materials were flocculated at fairly low salt concentrations in the fluid (LIN, 1987). These included kaolinite (median grain size 1 μm) and Cedar Key mud (2 μm). The others were flash I (14 μm), flyash II (10 μm), flyash III (14 μm), silica flour (7 μm) and Vicksburg loess (18 μm).

RESULTS

Front Behavior

As in the case of a non-settling salinity-induced gravity current, three distinct phases are found to occur during the movement of a turbidity front. These are characterized by different dominant driving forces, and are accordingly termed the initial adjustment phase, the inertial phase and the viscous phase (ROTTMAN and SIMPSON, 1983). These are shown for test COEL-5 (using kaolinite) in Figure 2, in which the front position, x_f, is plotted against elapsed time after gate opening. The three phases are marked by lines of different slopes. During the initial adjustment phase of unit line slope, the front propagated at a constant speed, driven by the initial density gradient between the main and closed-end channels. During the inertial phase of line slope 2/3, inertia and gravity forces dominated, and the front speed, dx_f/dt, was proportional to $-1/3$ power of time. For gravity currents, this $-1/3$ power dependence has been demonstrated both theoretically and experimentally by ROTTMAN and SIMPSON (1983). In the final, viscous phase, gravity and viscous forces entirely control front movement. The slope 0.29 is slightly higher than 1/

Table 1. *Summary of Test Conditions.*

Flume	L (m)	B (m)	H (cm)	C_o (mgL^{-1})	$\Delta\rho_1 \times 10^5$ (gcm^{-3})
WES	9.1	0.23	5.0 – 12.7	58 – 1878	1.6 – 74
COEL	14.7	0.10	8.0 – 10.6	250 – 3746	12 – 101

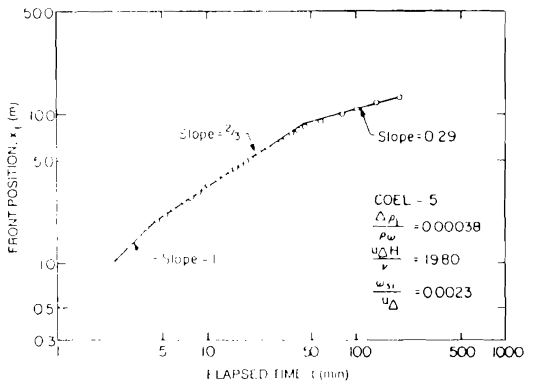

Figure 2. Front position with elapsed time after gate opening, test COEL-5.

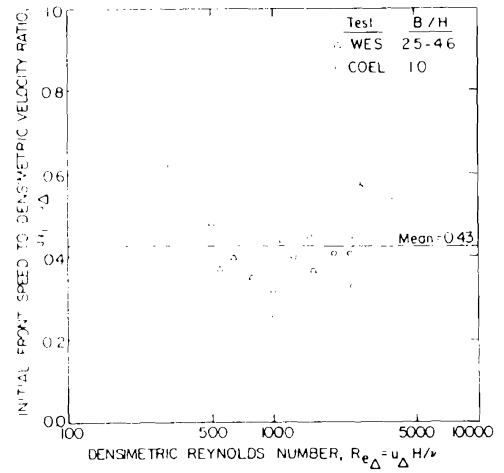

Figure 3. Dimensionless initial front speed against densimetric Reynolds number.

5 observed in a gravity current, partly because of stray effects from thermal gradients (LIN, 1987).

In several tests, the first phase was too short to be recorded. Furthermore, the point of transition from the second to the third phase was found to be highly dependent on the dimensionless settling velocity, w_{s1}/u_Δ. Thus for example in test COEL-5 characterized by w_{s1}/u_Δ = 0.0023, transition occurred at about 50 min after gate opening, while in test COEL-8 (using flyash III) with w_{s1}/u_Δ = 0.021, transition occurred at about 6 min. Thus in the latter case the relatively large particles settled out rapidly, leaving behind a slow moving very fine particle suspension influenced by viscous drag.

The dependence of the dimensionless initial front speed, u_{f1}/u_Δ, on the densimetric Reynolds number, Re_Δ, and the channel aspect ratio, B/H, suggested by dimensionless analysis (LIN, 1987) are examined using experimental data. Data plotted in Figure 3 from all the tests show a fair degree of scatter, but no easily defined trend of dependence of u_{f1}/u_Δ on either Re_Δ or B/H. Part of the reason for the scatter is believed to be the influence of the entrance gyre on front propagation. The gyre length in the x-direction was in the range of 0.2–0.4 m in WES tests and 0.1–0.2 m in COEL tests. Therefore, the front speed at x = 1 m in WES tests and 0.1–0.2 m in COEL tests. Therefore, the front speed at x = 1 m in WES tests and at x = 0.75 m in COEL tests (rather than x = 0) was conveniently selected as the initial front speed, u_{f1}. Notwithstanding data scatter, the mean value of u_{f1}/u_Δ is observed to be 0.43, which is fairly close to 0.46 obtained by KEULEGAN (1957, 1958) for salinity currents. A value of 0.50 can also be obtained theoretically based on the consideration of energy conservation (YIH, 1965). Since the effect of sediment settling is much less significant than that of the density gradient at the beginning, the correspondence between gravity and turbidity currents in this respect is not surprising (MIDDLETON, 1966).

Velocity Profiles

Illustrative results on the vertical velocity profiles at steady state corresponding to a sta-

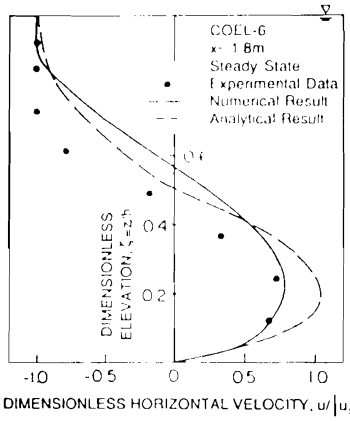

Figure 4. Dimensionless horizontal velocity profiles, test COEL-6 at x = 1.8 m.

tionary front are presented here. In Figure 4, the dimensionless horizontal velocity, $u/|u_s|$, is plotted against the dimensionless elevation, $\zeta = z/H$. The data are for test COEL-6 at x = 1.8 m. Self-similar profiles such as these occurred at every location within the front. However, the magnitude of the surface and bottom velocities decreased monotonically with distance. The flow velocities in the lower layer associated with relatively high concentration suspension caused the suspended material to move into the channel and deposit. Simultaneously, clear water left the channel through the upper layer.

Comparison has been made with numerical results as well as with analytically derived Eqs. 6 and 7. The numerical result is unaffected by the boundary layers due to the walls of the channel. The experimental data were obtained via a dye injection procedure in which the results were influenced both by the wall boundary drag and by lateral secondary currents. Limitations of the analytic solutions were noted previously. The numerical and analytic results satisfy the continuity requirement of equal discharge both ways.

Concentration Profiles

Suspension concentration at elevation z = 0.7 cm at five horizontal locations in test COEL-5 are plotted as a function of the elapsed time in Figure 5. At each location the elevation at which suspension concentration was measured was always below the corresponding interfacial elevation. The concentration is observed to rise from zero ahead of the moving front to an eventual steady state value. The time required to reach steady state after front passing increased with increasing distance, or with decreasing concentration. The concentration at steady state decreased with increasing distance because a certain amount of sediment had settled to the bottom. Numerical results compare reasonably well with the data.

Vertical concentration profiles for test COEL-5 are plotted at 67 and 190 min after gate opening in Figure 6. Five horizontal locations have been included. It is believed that a steady state had been attained prior to 67 min because of the nearly identical concentrations measured at the two different times at the same location. The well-mixed concentration profile at x = 0.1 m resulted from mixing within the entrance gyre. The magnitude of concentration decreased montonically from the entrance to the end of the front. It is noteworthy that in contrast with exponentially varying (with depth) suspension profiles in well-mixed open channel flows, the profiles in Figure 6 exhibit a uniform concentration in the lower portion of the profile. Agreement between data and numerical results (at 130 min) appears to be acceptable.

The exponential decay of mean concentration below the interface with distance and the influence of the dimensionless settling velocity, w_{s1}/u_Δ, on the longitudinal concentration distribution are apparent in Figure 7, in which the concentration ratio, $\bar{C}_b/\bar{C}_{b1}$ at steady state is plotted against dimensionless distance, x/H, on semi-logarithmic coordinates. Data from seven tests using kaolinite have been included. Three lines represented by different values of w_{s1}/u_Δ are shown. Line slope increases with increasing w_{s1}/u_Δ, since, for a given u_Δ, increasing w_{s1} implies increasing rate of deposition of sediment. These w_{s1}/u_Δ values were obtained by best fitting Eq. 8 to data using $\beta = 7$. As discussed by LIN (1987), the experimental results of GOLE *et al.* (1973) suggest this value of β to be reasonable. These w_1/u_Δ values differ from those based on measurement as given in the upper right hand corner of the figure. The discrepancy increases with increasing w_s/u_Δ as a result of inherent limitation in applying Eq. 8 to data using sediment with a rela-

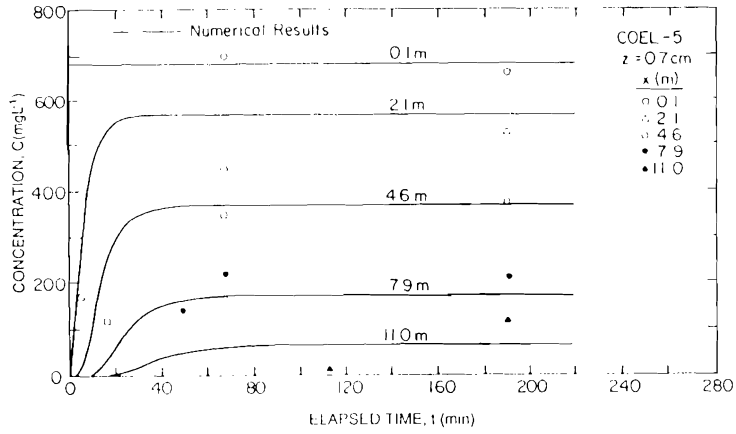

Figure 5. Suspension concentration at 0.7 cm elevation for five locations as a function of elapsed time after gate opening, test COEL-5.

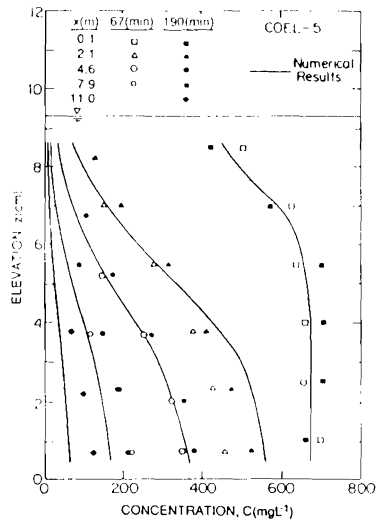

Figure 6. Suspension concentration profiles at steady state at five locations, test COEL-5.

tively large settling velocity. In such an event the vertical concentration gradient becomes pronounced. Hence the assumption of a uniform concentration in Eq. 8 is no longer reasonable.

Sediment Deposition and Influx

Sorting of deposited sediment was observed in all tests, with the grain size generally decreasing with distance from the entrance. The same trend has been reported in residential canals (WANLESS, 1975). For nearly cohesionless sediment such as flyash, sorting measurably increased with increasing w_{s1}/u_{Δ}.

The rate of deposition, δ, is plotted against distance from the entrance for test COEL-5 using kaolinite in Figure 8. δ is observed to decrease rapidly with distance, suggesting an exponential-type decay. Agreement between measurement and numerical prediction is acceptable, except for a slight over-prediction.

As noted the inflow velocity at the entrance reached a constant value shortly after gate opening. This velocity in conjunction with the entrance concentration resulted in sediment influx at a nearly constant rate during most of test duration. Thus the rate of sediment influx, S, can be practically calculated by dividing the total deposited sediment mass in the channel by the test duration and the area of the lower half of the flow cross-section at the entrance. The quantity, S, is plotted against entrance concentration, $\bar{C}_1$ in Figure 9. A 3/2 power dependence of S on $\bar{C}_1$ is clearly evident in accordance with Eq. 9. The coefficient 0.015 was calculated by selecting mean values of H = 8.8 cm and G_s = 2.55 for the twelve tests. The value α = 0.35, which is empirical, can be shown to be consistent with the observations of GOLE *et al.* (1973). The reasonable agreement between test data and prediction as illustrated in Figure 9 indicates that Eq. 9 can be used as a simple tool for

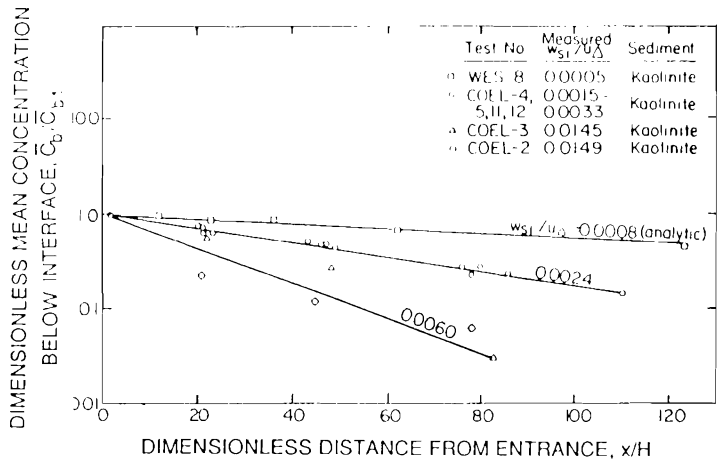

Figure 7. Dimensionless mean concentration below interface as a function of dimensionless distance, kaolinite tests.

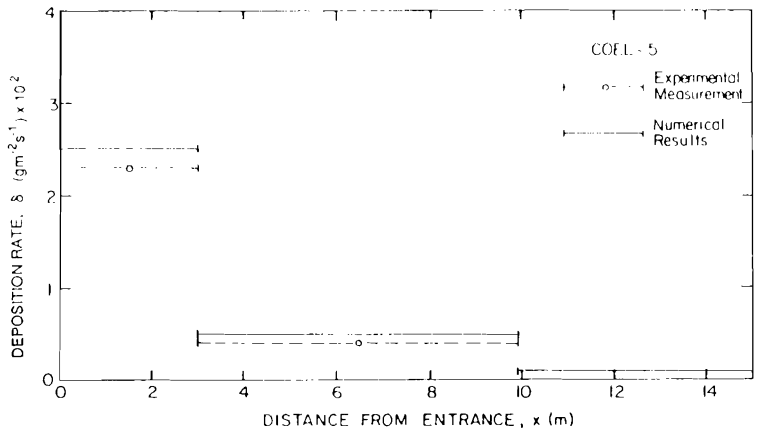

Figure 8. Variation of rate of deposition with distance, test COEL-5.9

the calculation of the rate of sedimentation in the channel.

CONCLUDING REMARKS

Some broad inferences derived from this study are noteworthy. The ratio of the sediment settling velocity to the densimetric velocity, w_{s1}/u_Δ, has been shown to be important in characterizing the combined effect of density gradient and sediment type on the turbidity current. There is an evident analogy with the well known formulations for (non-stratified) suspended sediment transport in which the settling velocity to friction velocity ratio is an important governing parameter. A conclusion is that notwithstanding similarities between the (depositional) turbidity current and non-settling gravity currents, the w_{s1}/u_Δ parameter highlights some basic differences between the two types of currents.

It is shown that the rate of sediment influx at steady state can be calculated via a relatively simple expression. The time-scale over which measurable sedimentation occurs in a closed-end channel is typically quite large in compar-

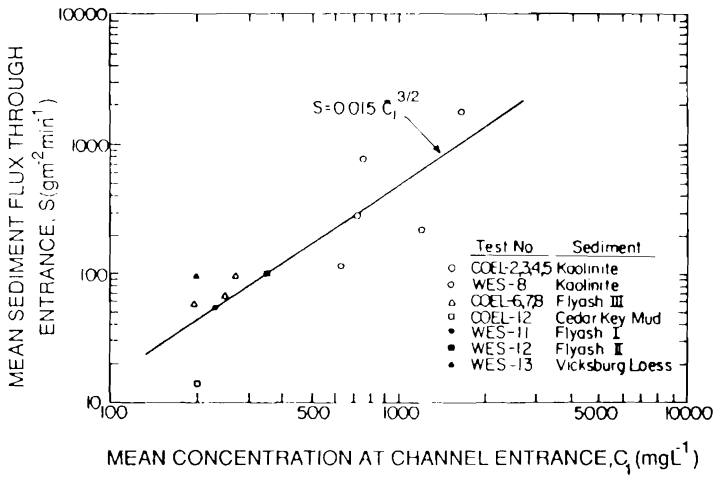

Figure 9. Mean sediment flux as a function of depth-mean concentration at the entrance.

ison with the time-response of the stationary front to, for example, changes in the concentration outside. Conceptually therefore it seems reasonable to represent the long-term sedimentation process as occurring under a series of stationary fronts at different values of the concentration outside. Under such conditions, Eq. 9 can be used to calculate cumulative sedimentation over a desired duration, *e.g.* a year.

To predict the flow and sediment concentration fields in a prototype closed-end channel at unsteady state, the two-dimensional numerical model developed in this study can be utilized. However, the coefficients involved in the model need to be determined by calibration using field data and independent laboratory measurements.

Finally, given Eq. 9, it is interesting to approximately estimate the relative contributions of turbidity current and tidal mass transport to sedimentation in coastal areas as follows.

The mass of sediment deposited, M_D, due to turbidity current over a tidal period T is equal to S(H/2)BT, neglecting tidal variation in H. Tide causes the sediment to be carried in during flood, a part of which deposits and the remainder is transported out during ebb. The mass deposited, M_T, is equal to $2\psi a_o LB\bar{C}_1$, where a_o is the tidal amplitude and $\psi \leq 1$ is the fraction of incoming sediment that deposits. For a given canal and tidal conditions, ψ strongly depends on the sediment settling velocity. The following ratio is now obtained:

$$\frac{M_T}{M_D} = 4\frac{\psi}{\alpha}\left(\frac{\Delta\rho_1}{\rho_w}\right)^{-1/2}\left(\frac{a_o}{H}\right)\left(\frac{L}{L'}\right) \qquad (10)$$

where $L' = T(gH)^{1/2}$ is the tidal wave length.

Consider a 1,000 m long and 5 m deep canal with a 0.5 m tidal amplitude and a semi-diurnal period. Assume $\Delta\rho_1/\rho_w = 10^{-3}$ and consider the canal to be a complete sediment trap, *i.e.* $\psi = 1$. Further assume $\alpha = 0.35$ to be applicable to this prototype canal. Under these conditions $M_T/M_D = 0.12$, which indicates the dominant effect of turbidity current in causing sedimentation in this case.

ACKNOWLEDGEMENT

Support from the National Science Foundation (Grant No. CEE-84-01490) and the Hydraulics Laboratory of the Waterways Experiment Station, Vicksburg, Mississippi is sincerely acknowledged.

LITERATURE CITED

AKIYAMA, J. and STEFAN, H., 1985. Turbidity current with erosion and deposition. *Journal of Hydraulic Engineering*, 111(12), December, 1473-1496.

BARR, D.I.H., 1963. Densimetric exchange flow in rectangular channels, I: Definitions, review and rel-

evance to model design. *La Houille Blanche*, 7, 739-753.

BENJAMIN, T.B., 1968. Gravity currents and related phenomena. *Journal of Fluid Mechanics*, 31(2), 209-248.

GOLE, C.V.; TARAPORE, Z.S. and GADRE, M.R., 1973. Siltation in tidal docks due to density currents. *In: Proceedings of the Fifteenth Congress of IAHR*, Volume 1, Istambul, Turkey, 335-340.

IPPEN, A.T. and HARLEMAN, D.R.F., 1952. Steady-state characteristics of subsurface flow. *Proceedings of Symposium on Gravity Waves*, Circular No. 521, National Bureau of Standards, Washington, DC, 79-93.

JENKINS, S.A.; INMAN, D.L. and BAILARD, J.A., 1980. Opening and maintaining tidal lagoons and estuaries. *In: Proceedings of the Seventeenth Coastal Engineering Conference*, ASCE, Volume II, Sydney, Australia, 1528-1547.

JOBSON, H.E. and SAYRE, W.W., 1970. Vertical transfer in open channel flow, *Journal of the Hydraulics Division*, 96(HY3), 703-724.

KEULEGAN, G.H., 1957. An experimental study of the motion of saline water from locks into fresh water channels. *Report No. 5168*, National Bureau of Standards, Washington, DC.

KEULEGAN, G.H., 1958. The motion of saline fronts in still water. *Report No. 5831*, National Bureau of Standards, Washington, DC.

KEULEGAN, G.H., 1966. The mechanism of an arrested saline wedge," *Estuary and Coastline Hydrodynamics*, Chapter 11 (Ippen, A.T., ed.). New York: McGraw-Hill, 546-574.

LIN, C.P., 1987. Turbidity currents and sedimentation in closed-end channels. Ph.D. Dissertation, University of Florida, Gainesville.

LIN, C.P. and MEHTA, A.J., 1986. Sediment-driven density fronts in closed end canals. *Physics of Shallow Estuaries and Bays*, Lecture Notes on Coastal and Estaurine Studies Series, Volume 16, (van de Kreeke, J., ed.). Berlin: Springer-Verlag, 259-276.

LOTT, J.W., 1986. Laboratory study on the behavior of turbidity current in a closed-end channel. *M.S. Thesis*, University of Florida, Gainesville.

McDOWELL, D.M., 1971. Currents induced in water by settling solids. In *Proceedings of the Fourteenth Congress*, IAHR, Volume 1, Paris, France, 191-198.

MEHTA, A.J. and MAA, P.-Y., 1985. Fine sedimentation in small harbor basins. In *Flocculation, Sedimentation & Consolidation*, (Moudgil, B.M., Somasundaran, P., eds.). New York: Engineering Foundation, 405-414.

MEHTA, A.J. and LOTT, J.W., 1987. Sorting of fine sediment during deposition. *Proceedings of Coastal Sediments '87*, ASCE, Volume 1, New Orleans, 348-362.

MIDDLETON, G.V., 1966. Experiments on density and turbidity currents. I. Motion of the head. *Canadian Journal of Earth Sciences*, 3, 523-546.

MILES, G.V., 1977. Formulation and development of a multi-layer model of estuarine flow. *Report No. INT 155*, Hydraulic Research Station, Wallingford, England.

O'BRIEN, M.P. and CHERNO, J., 1934. Model law for salt water through fresh. *Transactions*, ASCE, 576-609.

ROTTMAN, J.W. and SIMPSON, J.E., 1983. Gravity currents produced by instantaneous releases of a heavy fluid in a rectangular channel. *Journal of Fluid Mechanics*, 135, 95-110.

SIMPSON, J.E., 1972. Effect of the lower boundary on the head of a gravity current. *Journal of Fluid Mechanics*, 53, 757-768.

WANLESS, H.R. 1975. Sedimentation in canals. *Report*, Division of Marine Geology and Geophysics, Rosenstiel School of Marine and Atmospheric Science, University of Miami, Miami, Florida.

YIH, C.S., 1965. *Dynamics of Nonhomogeneous Fluids*, New York: Macmillan.